Available online at www.sciencedirect.com

ScienceDirect

IFAC Papers Online CONFERENCE PAPER ARCHIVE

IFAC PapersOnLine 59-22 (2025) 237–242

Energy efficient control of electric driven vessels including current effects

Pia-Lucia Jonitz, * **Thomas Meurer** *

* *Karlsruhe Institute of Technology (KIT), Institute of Mechanical Process Engineering and Mechanics, 76131 Karlsruhe, Germany (e-mail:{pia-lucia.jonitz, thomas.meurer}@kit.edu).*

Abstract: Energy consumption and emissions in shipping are playing an expanding role due to their impact on climate change. Combined with the shortage of nautical staff, automation and autonomy concepts move into the focus. Autonomous ships offer the opportunity to increase energy efficiency through intelligent control and trajectory planning. Given the example of an electric driven vessel it is shown how energy demands can be reduced by taking disturbances, such as water currents, into account in trajectory planning. For this, trajectory tracking is performed with a model predictive control approach. Therefore, an overall model of the ship with two effectors that are operated by electric drives (actuators) as an alternative to diesel or gasoline engines is used. The energy demand is investigated on the basis of the energy level of a high voltage battery that delivers the power to electrical machines.

Keywords: Autonomous vessel, energy consumption, electric vessel, potential field, model predictive control, trajectory tracking, trajectory planning

1. INTRODUCTION

Autonomous shipping has become an important aspect in the maritime industry. With climate change, energy efficiency plays an increasing role. As a consequence many path-planning algorithms, in addition to safety, incorporate energy-related criteria. In Garau et al. (2009) and in Teong-Beng Koay (2013) a path planning based on A* is proposed using sea current data to calculate energy-optimal paths. In Krell et al. (2022) a particle swarm optimization is used to obtain energy-efficient and reward-based path planning, and in Luo et al. (2024) a gradient descent method is implemented to find an energy-efficient path in a previously created energy weight map. In Zhu et al. (2025) an energy-efficient route planning based on level-set methods is shown. These sources have in common that the ship is approximated by a point mass or a non-model-based approach is used. Furthermore, the energy consumption is approximated by a simple model depending on the difference between the vessel and water current velocity.

To address a more realistic setup, in this paper, a 3DOF dynamic motion model of the vessel is used and environmental forces are mapped to the vessel geometry. Trajectory planning is performed by solving an optimal control problem in which reducing energy consumption is part of the cost function. Furthermore, the flow field is in contrast to the presented sources modeled as a force field instead of a velocity field. Motivated by the theory of potential flow in Birk (2019) this is realized by artificial potential fields (APF), which are typically utilized to avoid obstacles. The classical concept is to create a virtual potential field around the vehicle in which attractive forces lead the vehicle to the target and repulsive forces keep it away from obstacles (Khatib, 1986). In Wang and Im (2024), Luo et al. (2024) and in Suo et al. (2024) this method is used for obstacle avoidance in the context of autonomous shipping. To validate energy demand reduction a trajectory tracking algorithm for an electric vessel is developed and evaluated.

The control of an over-actuated vessel with a redundant set of effectors and actuators typically includes several levels. First, a high-level motion control instructs a vector of virtual forces and torques to realize the overall motion control objectives. Second, the control allocation solves an optimization problem so that the effectors provide the desired virtual control performance (Johansen and Fossen, 2013). This approach is used in Bradner (2014), Torben et al. (2019), Kosch et al. (2022) and Skulstad et al. (2023). In the control allocation, a second objective is to increase the efficiency of the power conversion (Johansen and Fossen, 2013). In Bradner (2014) the minimization of power is part of the cost function for control allocation. In this paper, trajectory tracking and power minimization is realized in only one level by using a model predictive control approach. This has the advantage that constraints for the effectors can be considered directly and the dynamics of actuators is not ignored. The energy demand will be investigated by comparing the energy level of a battery, which delivers the power for the electrical machines that drives the effectors. Electrification is motivated in general by the energy transition and in particular by already existing electrified ferries, see, e.g., Prevljak (2025). This reference also motivates the dimensions of the power train system used subsequently.

The paper is structured as follows. In Section 2 the dynamic motion model is described. The current forces represented using potential fields are introduced and mapped to the geometry of the ship. Section 3 introduces the control design methods. The results based on two example

2405-8963
Peer review under responsibility of International Federation of Automatic Control.
10.1016/j.ifacol.2025.11.638

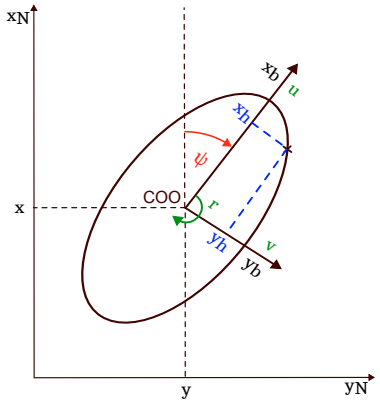

Fig. 1. Vessel position and orientation in NED frame and velocities in body-fixed frame for 3DOF surface vessel.

maneuvers are presented in Section 4. Finally, in Section 5 a conclusion of the paper is provided.

2. MATHEMATICAL MODELING

The dynamic model of the vessel extended by the propulsion system with the electric machine and battery are introduced and current-induced forces are integrated as disturbances.

2.1 Vessel dynamics

Under calm sea conditions the vessel's dynamics can be described by a 3DOF model. Surge and sway velocities and the yaw rate are described by $\boldsymbol{v} = [u,\, v,\, r]^T$ in the body-fixed coordinate system of the ship. The position of the center of origin (COO) of the vessel in the North-East-Down (NED) frame is $\boldsymbol{\eta} = [x,\, y,\, \psi]^T$, where x and y correspond to the north and east coordinate, respectively, and ψ describes the orientation with respect to the north axis (Fossen, 2011). This is illustrated in Fig. 1. The transformation between the coordinate systems reads

$$\dot{\boldsymbol{\eta}} = R(\psi)\boldsymbol{v} \qquad R \in \mathrm{SO}(3), \tag{1}$$

where $R(\psi)$ denotes the rotation matrix relating the body fixed and the NED frame. With this, the dynamic motion of the vessel is given in the form

$$M\dot{\boldsymbol{v}} + \big(C(\boldsymbol{v}) + D(\boldsymbol{v})\big)\boldsymbol{v} = \boldsymbol{\tau}(\boldsymbol{u}) + \boldsymbol{\tau}_{\mathrm{env}}(\boldsymbol{\eta}). \tag{2}$$

These equations can be derived by using Newton's second law. For details the reader is referred to Fossen (2011). The system inertia $M = M_{RB} + M_A$ is determined by the rigid body mass matrix M_{RB} and the added mass matrix M_A, which is caused by hydrodynamic forces. The Coriolis matrix $C(\boldsymbol{v})$ contains contributions from the rotation of the vessel about the inertial frame and hydrodynamic added Coriolis and centripetal effects. The damping matrix $D(\boldsymbol{v})$ captures potential damping, possible skin friction, and quadratic or higher-order damping terms. Model parameters from Skjetne (2005) are taken, normalized, and then scaled up using the bis-system (Fossen, 2011). The scaled vessel is $L = 40\,\mathrm{m}$ long, $b = 10\,\mathrm{m}$ wide and has a mass of 260 tons. The center of gravity (COG) is set to the COO of the vessel. The vector $\boldsymbol{\tau}_{\mathrm{env}}(\boldsymbol{\eta}) = [X_{\mathrm{env}}(\boldsymbol{\eta}),\, Y_{\mathrm{env}}(\boldsymbol{\eta}),\, N_{\mathrm{env}}(\boldsymbol{\eta})]^T$ in (2) describes environmental forces in the body-fixed coordinate system depending on the actual position $\boldsymbol{\eta}$ in the NED frame.

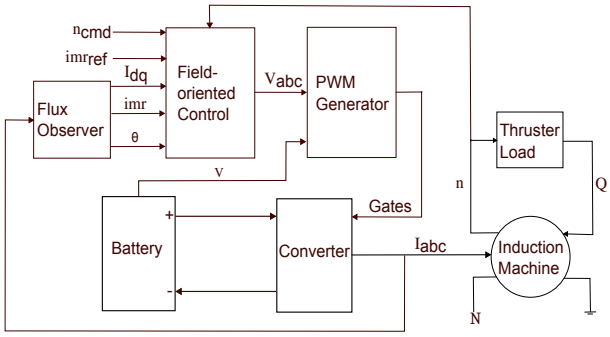

Fig. 2. Structure of power train system for one thruster.

The input force vector $\boldsymbol{\tau}(\boldsymbol{u})$ depends on the inputs $\boldsymbol{u}$ of the installed effectors.

2.2 Propulsion dynamics

The considered effectors at the ship are two azimuth thrusters. The produced force can be approximated with

$$T_i(n_i) = \rho D^4 K_T |n_i| n_i \quad i = 1, 2 \text{ (number of thrusters)},$$

where D is the thruster diameter, which is 1.3 m, ρ is the density of the water, n_i is the rotational speed, and K_T is a thruster specific coefficient depending on the blade area ratio, the diameter, and the number of blades of the thruster (Barnitsas et al., 1981). Since an azimuth thruster can be rotated around its axis the forces in surge (T_{xi}) and sway (T_{yi}) direction in the body fixed coordinate system can be expressed with the angle of rotation α_i by

$$\begin{bmatrix} T_{x_i}(\alpha_i, n_i) \\ T_{y_i}(\alpha_i, n_i) \end{bmatrix} = \begin{bmatrix} \cos(\alpha_i) \\ \sin(\alpha_i) \end{bmatrix} T_i(n_i) \quad i = 1, 2$$

With the positions l_{x_i}, l_{y_i} of the effectors on the vessel, the forces and the moment acting in the COG of the vessel are

$$\boldsymbol{\tau}(\boldsymbol{u}) = \begin{bmatrix} 1 & 0 & 1 & 0 \\ 0 & 1 & 0 & 1 \\ -l_{y_1} & l_{x_1} & -l_{y_2} & l_{x_2} \end{bmatrix} \begin{bmatrix} T_{x_1}(\alpha_1, n_1) \\ T_{y_1}(\alpha_1, n_1) \\ T_{x_2}(\alpha_2, n_2) \\ T_{y_2}(\alpha_2, n_2) \end{bmatrix}. \tag{3}$$

Herein $\boldsymbol{u} = [\alpha_1,\, n_1,\, \alpha_2,\, n_2]^T$ serves as the input of the effectors. The dynamics of the actuators are not static as it is often mentioned (Johansen and Fossen, 2013). Hence, the rotational speed n_i and the azimuth angle α_i depend on time t. The angle is normally adjusted by a servo motor, whose dynamics is faster than the one of the thrusters and thus can be approximately neglected or assumed with a sufficiently smaller time constant.

2.3 Power train system

Fig. 2 summarizes the structure of the power train system. The power to drive the thrusters is delivered by two squirrel-cage induction motors with 500 kW each. The ideal load torque of the respective machine

$$Q_i(n_i) = \rho D^5 K_Q |n_i| n_i \qquad i = 1, 2$$

depends on the used thruster. Here K_Q is a thruster-specific coefficient. A field-oriented control (FOC) is implemented for the electric machine. The basic idea of FOC is to select a reference system that rotates with the flux space vector. (Llorente, 2020) The flux observer is used to estimate the actual magnetic rotor flux imr and the reference angle θ, which is needed to transform the sinusoidal

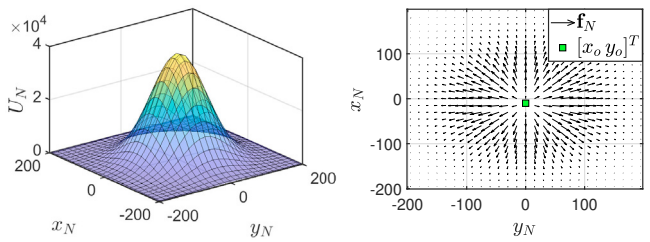

Fig. 3. Potential field and corresponding virtual force field.

system with alternating currents $\boldsymbol{I}_{abc} = [i_a,\, i_b,\, i_c]^T$ into the constant system with direct currents $\boldsymbol{I}_{dq} = [i_d,\, i_q]^T$. Herein i_d is the field forming and i_q the torque forming component. In the FOC block in Fig. 2 a cascade of PI-controllers determines the voltage $\boldsymbol{U}_{dq} = [u_d,\, u_q]^T$, which can be transformed back in the sinusoidal system by using θ. A pulse width modulation (PWM) generator then creates the input signals for the B6 bridge of the converter. This converter transforms the DC from the high-voltage battery according to the gate requirement into $\boldsymbol{I}_{abc}$ for the electric machine, so that it realizes the required rotational speed. Due to the FOC the step response of the power train system with the requested rotational speed $n_{i,\mathrm{cmd}}$ as input and the resulting rotational speed n_i as output shows PT_1 behavior. This admits a simplified representation in terms of the linear system

$$\dot{\boldsymbol{u}} = A\boldsymbol{u} + B\boldsymbol{u}_{\mathrm{cmd}}, \quad \boldsymbol{u}(0) = \boldsymbol{u}_0 \in \mathbb{R}^4 \tag{4}$$

with $\boldsymbol{u}_{\mathrm{cmd}} = [\alpha_{1,\mathrm{cmd}},\, n_{1,\mathrm{cmd}},\, \alpha_{2,\mathrm{cmd}},\, n_{2,\mathrm{cmd}}]^T$ and the matrices A and B determined by parameter identification to fit the observed closed loop response of the detailed power train model. The battery is assumed to have a capacity of 900 kWh and its charging level is considered to be in the interval between 40 % and 80 %, where the discharging curve can be linearly approximated (Aneiros et al., 2013).

2.4 Modeling environmental forces

In the potential field method the virtual forces are typically modeled by torsion-free fields, which can be computed by building the gradient of a potential field. For illustration purposes subsequently the potential field $U_N = ab\,\mathrm{e}^{-((x_N-x_o)^2+(y_N-y_o)^2)/(2b)}$ centered at (x_o, y_o) is used, see Fig. 3 (left). By calculating the gradient $\boldsymbol{f}_N = -\nabla U_N$ the force vector field in the NED frame is obtained as

$$\boldsymbol{f}_N = \begin{bmatrix} f_{N,x} \\ f_{N,y} \end{bmatrix} = \begin{bmatrix} (x_N - x_o) \\ (y_N - y_o) \end{bmatrix} \frac{U_N}{b}.$$

This vector field is illustrated in Fig. 3 (right) and is used to simulate environmental forces. The parameters a, b define the force maximum and shape. To build-up complex scenarios, several force vector fields generated from potential fields $U_{N,i},\ i = 1, ..., m$ can be added to obtain $\boldsymbol{f}_N = -\sum_{i=1}^{m} \nabla U_{N,i}$. If the ship enters the field, then the virtual forces act on the side facing the force. Therefore in the next step the generated force on the ship side is determined. The ship hull in the NED frame can be described by

$$[x_N\ \ y_N]^T = [x\ \ y]^T + R(\psi)[x_h\ \ y_h]^T, \quad R \in \mathrm{SO}(2) \tag{5}$$

according to Fig. 1. For simplicity and as commonly used, the hull is approximated by an ellipse. Hence by parameterizing x_h and y_h the curve describing the ellipse

$$\boldsymbol{s}_h(p) = \begin{bmatrix} x_h(p) \\ y_h(p) \end{bmatrix} = \frac{1}{2} \begin{bmatrix} L \sin(p) \\ b \cos(p) \end{bmatrix}, \quad 0 \le p \le 2\pi \tag{6}$$

is obtained. To evaluate the total force vector $\boldsymbol{F}_N$ along the vessel's hull C the curve integral

$$\boldsymbol{F}_N = \int_C \boldsymbol{f}_N \mathrm{ind}(x_N, y_N) \mathrm{d}s$$

needs to be solved. Herein the indicator function

$$\mathrm{ind}(x_N, y_N) = \begin{cases} 1, & \langle \boldsymbol{f}_N, \boldsymbol{n}_N \rangle \le 0 \\ 0, & \langle \boldsymbol{f}_N, \boldsymbol{n}_N \rangle > 0 \end{cases}$$

is used, where the scalar product $\langle \boldsymbol{f}_N, \boldsymbol{n}_N \rangle$ with $\boldsymbol{n}_N$ the outer normal vector of $\boldsymbol{s}_h(p)$ in the NED frame is needed to distinguish if $\boldsymbol{f}_N$ affects the vessel or not. The normal vector of $\boldsymbol{s}_h(p)$ in the body frame thereby reads

$$\boldsymbol{n}_h = \frac{1}{2} \begin{bmatrix} b \sin(p) \\ L \cos(p) \end{bmatrix}.$$

Similar to (5) the normal vector $\boldsymbol{n}_N$ in the NED frame reads $\boldsymbol{n}_N = R(\psi)\boldsymbol{n}_h$. With the ellipse shaped vessel geometry in the NED frame

$$\boldsymbol{s}_N(p, \boldsymbol{\eta}) = [x\ \ y]^T + R(\psi)\boldsymbol{s}_h(p)$$

evaluated by combining (5) and (6) the integral is transformed into the following form

$$\boldsymbol{F}_N(\boldsymbol{\eta}) = \int_0^{2\pi} \boldsymbol{f}_N(\boldsymbol{s}_N(p, \boldsymbol{\eta})) |\boldsymbol{s}'_N(p, \boldsymbol{\eta})| \mathrm{ind}(p, \boldsymbol{\eta}) \mathrm{d}p$$

by using the functional determinant $|\boldsymbol{s}'_N(p, \boldsymbol{\eta})|$. With the two dimensional rotation matrix $R(\psi)$ in

$$\begin{bmatrix} X_{\mathrm{env}}(\boldsymbol{\eta}) \\ Y_{\mathrm{env}}(\boldsymbol{\eta}) \end{bmatrix} = R^{-1}(\psi) \boldsymbol{F}_N(\boldsymbol{\eta}) \tag{7}$$

the forces are transformed into the body coordinate system. The torque generated by the force field acting on the ship hull is the cross product of force and lever arm. Hence, the torque in the COG for one point on the hull can be evaluated with the force vector in the body frame acting on the ship hull and the point of attack $\boldsymbol{p}_h = [x_h,\, y_h]^T$ with

$$N_h = R^{-1}(\psi) \boldsymbol{f}_N(\boldsymbol{s}_N(p, \eta)) \times \boldsymbol{p}_h.$$

The total torque along the curve is obtained as previously derived by evaluating the integral

$$N_{\mathrm{env}}(\eta) = \int_0^{2\pi} N_h(\boldsymbol{s}_N(p, \boldsymbol{\eta})) |\boldsymbol{s}'_N(p, \boldsymbol{\eta})| \mathrm{ind}(p, \boldsymbol{\eta}) \mathrm{d}p.$$

These preparations imply

$$\boldsymbol{\tau}_{\mathrm{env}}(\boldsymbol{\eta}) = [X_{\mathrm{env}}(\boldsymbol{\eta})\ \ Y_{\mathrm{env}}(\boldsymbol{\eta})\ \ N_{\mathrm{env}}(\boldsymbol{\eta})]^T, \tag{8}$$

which is included in (2). The added value of modeling the current with a force field instead of a velocity field can be seen here. First, the force along the hull of the vessel can be evaluated and thus a more realistic behavior can be achieved. Second, forces and moments can be directly included into $\boldsymbol{\tau}_{\mathrm{env}}(\boldsymbol{\eta})$ in the vessel model, while current velocities $\boldsymbol{v}_c$ have to be considered in the damping and Coriolis terms of the 3DOF model.

To identify the force field acting on the ship in real world, the drag force can be calculated using forecast current data as in Teong-Beng Koay (2013). As an alternative the estimation method presented in Kosch (2023) could be used, which generates a continuously adapting current velocity map based on measurements from a vessel-mounted current sensor.

3. OPTIMAL CONTROL DESIGN

The control part is split up in to two subproblems: First an vessel trajectory is computed by solving an optimal control problem and second, this trajectory is tracked using a nonlinear MPC (NMPC). This approach is motivated by performing trajectory planning for the more involved system taking into account the vessel dynamics and the environmental forces offline to reduce the computational burden for the online NMPC. The latter is setup up to directly include the control allocation and to use the power train system to evaluate the power consumption.

3.1 Trajectory planning

To outline the added value of taking into account environmental forces the optimal trajectories are planned by considering the cost functional

$$\min_{\boldsymbol{\tau}} J = \int_0^T \boldsymbol{\tau}^T R \boldsymbol{\tau} \, \mathrm{d}t \tag{9a}$$

penalizing the input forces $\boldsymbol{\tau}$ and thus energy consumption along the trajectory. Dynamic constraints are added by (1) and (2), i.e.,

$$\begin{bmatrix} \dot{\boldsymbol{\eta}} \\ \dot{\boldsymbol{v}} \end{bmatrix} = \begin{bmatrix} R(\psi)\boldsymbol{v} \\ M^{-1}\big[(-C(\boldsymbol{v}) - D(\boldsymbol{v}))\boldsymbol{v} + \boldsymbol{\tau} + \beta \boldsymbol{\tau}_{\mathrm{env}}(\boldsymbol{\eta})\big] \end{bmatrix} \tag{9b}$$

with $\beta \in \{0, 1\}$ to switch the effect of environmental forces according to Section 2.4 on or off. Equality and inequality constraints

$$\boldsymbol{\eta}(0) = \boldsymbol{\eta}_0,\, \boldsymbol{v}(0) = \boldsymbol{v}_0,\, \boldsymbol{\eta}(T) = \boldsymbol{\eta}_T,\, \boldsymbol{\tau}_{\min} \leq \boldsymbol{\tau} \leq \boldsymbol{\tau}_{\max} \tag{9c}$$

are added to include start and target points as well actuation constraints. Based on a full discretization an SQP algorithm is used to solve (9) to provide the optimal (open-loop) input $\boldsymbol{\tau}_{\mathrm{opt}}$ and the corresponding trajectory $\boldsymbol{\eta}_{\mathrm{opt}}$.

3.2 Trajectory tracking

Trajectory tracking is realized by solving the optimal control problem

$$\begin{aligned} \min_{\boldsymbol{u}_{\mathrm{cmd}}} J = \int_0^{T_p} \Big\{ & \gamma_1 \|\boldsymbol{\eta}(t) - \boldsymbol{\eta}_{\mathrm{opt}}(t)\|^2 \\ & + \gamma_2 \|\boldsymbol{n}_{\mathrm{cmd}}(t)\|^2 + \gamma_3 \|\boldsymbol{\tau}(\boldsymbol{u}(t)) - \boldsymbol{\tau}_{\mathrm{opt}}(t)\|^2 \Big\} \mathrm{d}t \end{aligned} \tag{10a}$$

with $\boldsymbol{n}_{\mathrm{cmd}} = [n_{1,\mathrm{cmd}},\, n_{2,\mathrm{cmd}}]^T$ subject to

$$\begin{bmatrix} \dot{\boldsymbol{\eta}} \\ \dot{\boldsymbol{v}} \\ \dot{\boldsymbol{u}} \end{bmatrix} = \begin{bmatrix} R(\psi)\boldsymbol{v} \\ M^{-1}\big[(-C(\boldsymbol{v}) - D(\boldsymbol{v}))\boldsymbol{v} + \boldsymbol{\tau}(\boldsymbol{u})\big] \\ A\boldsymbol{u} + B\boldsymbol{u}_{\mathrm{cmd}} \end{bmatrix} \tag{10b}$$

and equality as well as inequality constraints

$$\begin{aligned} & \boldsymbol{\eta}(0) = \boldsymbol{\eta}_0,\, \boldsymbol{v}(0) = \boldsymbol{v}_0, \boldsymbol{u}(0) = \boldsymbol{u}_0, \\ & \boldsymbol{n}_{\min} \leq \boldsymbol{n}_{\mathrm{cmd}} \leq \boldsymbol{n}_{\max},\, \dot{\boldsymbol{u}}_{\min} \leq\ \dot{\boldsymbol{u}}_{\mathrm{cmd}} \leq \dot{\boldsymbol{u}}_{\max} \end{aligned} \tag{10c}$$

on a receding horizon T_p, see, e.g., Camacho and Bordons (2007) for an introduction to MPC. The resulting control signal $\boldsymbol{u}_{\mathrm{cmd}}$ is applied over the control horizon T_c and the initial states $\boldsymbol{\eta}_0$, $\boldsymbol{v}_0$, $\boldsymbol{u}_0$ are updated. The dynamic model (10b) includes the dynamics of the actuators (4) as described in Section 2.2. The cost functional contains three terms. First, the error between the actual pose $\boldsymbol{\eta}$ and its reference $\boldsymbol{\eta}_{\mathrm{opt}}$. Second, as the energy requirement on the battery depends bi-quadratically on the rotational speed $n_{i,\mathrm{cmd}}$, $i = 1, 2$, both values are penalized. The third term allows to include the control allocation. Since a one level solution is sought here due to including the power train directly $\gamma_3 = 0$ is set. The inequality constraints in (10c) refer to the maximal (minimal) rotational speeds and rate constraints of the commanded input $\boldsymbol{u}_{\mathrm{cmd}}$.

4. SIMULATION RESULTS

In this section simulation results are presented for two maneuvers involving environmental forces, i.e., (8). The OCP for trajectory planning and the NMPC for the trajectory tracking task are implemented and solved in MATLAB using a multiple shooting method combined with an SQP algorithm. Here, the state and the input vector are parametrized as piecewise constant. The power train system is built using Simulink.

4.1 Trajectory planning

Maneuver 1 is planned from $\boldsymbol{\eta}_0 = [0\,\mathrm{m},\, 100\,\mathrm{m},\, 0°]^T$ to the position $\boldsymbol{\eta}_T = [200\,\mathrm{m},\, 0\,\mathrm{m},\, -90°]^T$ for $T = 200$ s. The origin of the single potential field is placed at $x_o = -10\,\mathrm{m}$, $y_o = 0\,\mathrm{m}$. Maneuver 2 (Fig.4 on the right) is planned from $\boldsymbol{\eta}_0 = [0\,\mathrm{m},\, 100\,\mathrm{m},\, 0°]^T$ to the position $\boldsymbol{\eta}_T = [250\,\mathrm{m},\, -100\,\mathrm{m},\, 0°]^T$ with an additional second potential field centered at $x_o = 250\,\mathrm{m}$, $y_o = 100\,\mathrm{m}$. Furthermore, the vessel is assumed to start from rest $\boldsymbol{v}_0 = \boldsymbol{0}$. The obtained trajectories from solving (9) are shown in Fig. 4 for Maneuver 1 (left) and Maneuver 2 (right). Red curves and snapshorts refer to the case $\beta = 0$, i.e., environmental forces are neglected, while the blue curves to the case $\beta = 1$, where environmental forces are included. The difference between the red and the blue trajectories become immediately apparent for both maneuvers. As it can be seen, the trajectory (in blue) involving $\boldsymbol{\tau}_{\mathrm{env}}(\eta)$, either avoids large force contributions or exploits them to reach the target.

4.2 Trajectory tracking

To evaluate the NMPC the simulation model is extended by the environmental forces as disturbances, i.e., (1), (2) with (8) and (4) are used to model the plant. For the numerical solution, a sampling time $T_s = 1$ s and a simulation time for 200 s are used. Prediction and control horizon are set to $T_p = 30$ s and $T_c = T_s$. The control input is assumed to be piecewise constant. Figures 5 and 6 present the results of the trajectory tracking with the NMPC for both maneuvers. The orange arrows indicate the direction of the effector forces at three positions of the vessel. Red colors refer to the planned reference trajectory and pose while blue colors denote the resulting trajectory and pose from the solution of the NMPC. Notably, rather accurate trajectory tracking is achieved for both maneuvers without assuming the availability of the environmental forces $\boldsymbol{\tau}_{\mathrm{env}}(\eta)$ in the NMPC. The comparison between the trajectory planning and the trajectory tracking, however, reveals differences in the respective vessel orientation.

4.3 Comparison of energy demands

To compare the energy requirements, the driving profiles of the maneuvers are simulated using the power train system

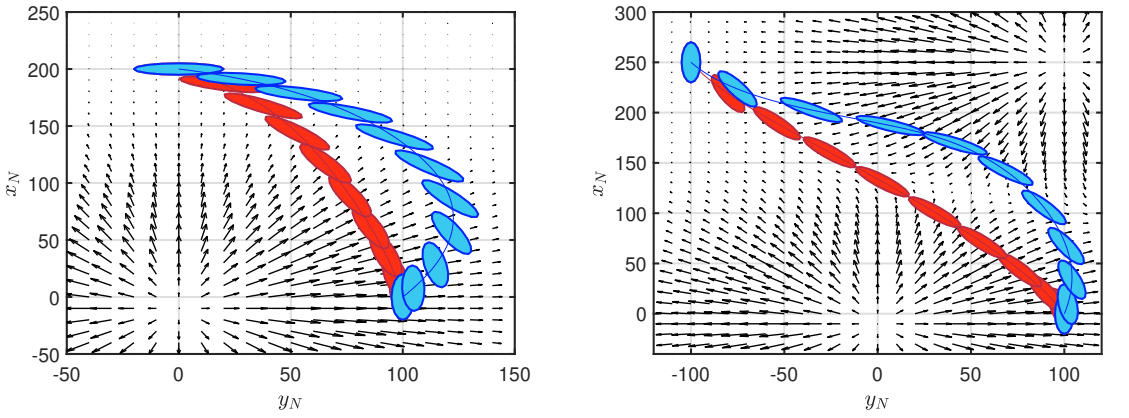

Fig. 4. Planned trajectories for Maneuver 1 (left) and Maneuver 2 (right) from (9) for $\beta = 0$ (red) and $\beta = 1$ (blue).

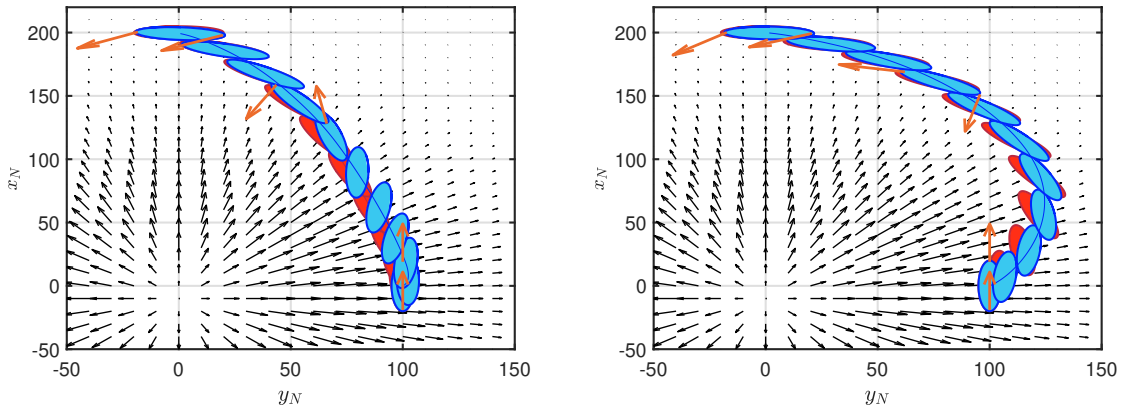

Fig. 5. Trajectory tracking for Maneuver 1 with the direction of the effector forces exemplarily outlined at three time steps (orange arrows). Reference (red) trajectory and pose from the solution of (9) with $\beta = 0$ (left) and $\beta = 1$ (right) compared to the NMPC trajectory and pose (blue).

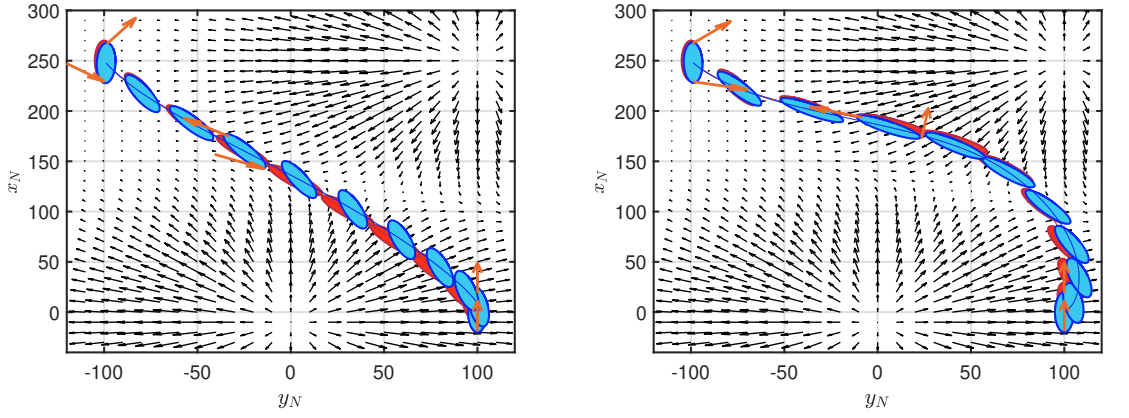

Fig. 6. Trajectory tracking for Maneuver 2 with the direction of the effector forces exemplarily outlined at three time steps (orange arrows). Reference (red) trajectory and pose from the solution of (9) with $\beta = 0$ (left) and $\beta = 1$ (right) compared to the NMPC trajectory and pose (blue).

described in Section 2.3. The reference input for the FOC of the electric machines is the required rotational speed $n_{i,\mathrm{cmd}}$, $i = 1, 2$ computed by the NMPC in Section 3.2. The energy demand is assessed by monitoring the state of charge of the batteries. This energy demand provided by the two batteries (one for each drive) is depicted in Fig. 7. As expected the energy requirement for tracking the trajectory computed without considering $\boldsymbol{\tau}_{\mathrm{env}}(\eta)$ is significantly higher. By calculating the relative energy savings, it is determined that the energy requirements are reduced by about 60 % for both maneuvers if the environmental forces are taken into account for trajectory planning, The numerical evaluation of other maneuvers indicates that these savings depend on the planned route

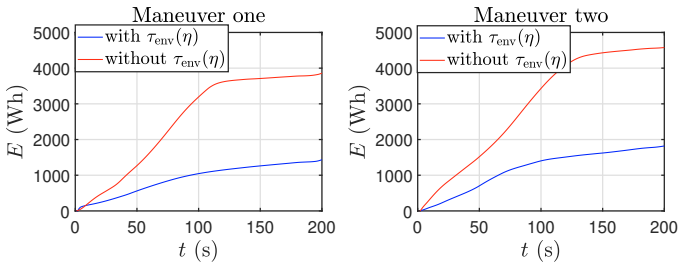

Fig. 7. Energy consumption of the batteries.

and the proximity of the vessel to the strongest forces in the field and vary between 10 % and 65 %. In summary, a range extension can be achieved if environmental forces are taken into account for trajectory planning. This, however, requires either measurement data by mounted or floating sensors, additional disturbance estimators that can be based on the setup shown in Section 2.4 or data-based forecasting approaches.

5. CONCLUSIONS

Optimal trajectory planning and trajectory tracking using NMPC are considered for an electrified vessel with battery. For this the vessel dynamics is complemented by the model of the propulsion system and the power train. Moreover, environmental forces resulting from the current effects are captured by following a potential fields approach. It is shown in a simulation study that the presented approach provides a high robustness of trajectory tracking in view of environmental disturbances. To evaluate the energy consumption and thus the possible range of operation the driving profile is assessed using the power train model. The observed savings motivate the utilization of environment (forecasting) models for trajectory planning. Future work will address the inclusion of real environmental data in terms of flow patterns and the incorporation of model- and data-based forecasting approaches into the control setup.

REFERENCES

Aneiros, E., Lobo, D., López, A., and Álvarez, R. (2013). A proposed mathematical model for discharge curves of Li-Ion batteries. In *2013 International Conference on New Concepts in Smart Cities: Fostering Public and Private Alliances (SmartMILE)*, 11–13. IEEE. doi:10.1109/SmartMILE.2013.6708177.

Barnitsas, M.M., Ray, D., and Kinley, P. (1981). Kt, Kq and Efficiency Curves for the Wageningen B-Series Propellers. *University of Michigan*.

Birk, L. (2019). *Fundamentals of Ship Hydrodynamics*. doi:10.1002/9781119191575.

Bradner, A. (2014). *Optimale Allokation für Voith-Schneider Propeller im Rahmen des dynamischen Positionierens*. Ph.D. thesis, Faculty of Mathematics and Economics at the University of Ulm.

Camacho, E.F. and Bordons, C. (2007). *Model Predictive Control*. Springer, London, England, UK.

Fossen, T.I. (2011). *Handbook of Marine Craft Hydrodynamics and Motion Control*. Wiley. doi:10.1002/9781119994138.

Garau, B., Bonet, M., Alvarez, A., Ruiz, S., and Pascual, A. (2009). Path Planning for Autonomous Underwater Vehicles in Realistic Oceanic Current Fields: Application to Gliders in the Western Mediterranean Sea. *Journal of Maritime Research*, 6, 5–22.

Johansen, T. and Fossen, T. (2013). Control allocation—A survey. *Automatica*, 49, 1087–1103. doi:10.1016/j.automatica.2013.01.035.

Khatib, O. (1986). Real-Time Obstacle Avoidance for Manipulators and Mobile Robots. *Int. J. Rob. Res.*, 5(1), 90–98. doi:10.1177/027836498600500106.

Kosch, M. (2023). *Online trajectory generation and tracking control for automated river ferries*. Ph.D. thesis, Rheinisch-Westfälische Technische Hochschule Aachen, Aachen.

Kosch, M., Koschorrek, P., and Abel, D. (2022). A Reference Trajectory-Based Approach to Safe and Efficient Trajectory Planning for an Overactuated River Ferry. *IFAC-PapersOnLine*, 55(31), 31–36. doi:10.1016/j.ifacol.2022.10.405.

Krell, E., King, S.A., and Garcia Carrillo, L.R. (2022). Autonomous Surface Vehicle energy-efficient and reward-based path planning using Particle Swarm Optimization and Visibility Graphs. *Appl. Ocean Res.*, 122, 103125. doi:10.1016/j.apor.2022.103125.

Llorente, R.M. (2020). *Practical Control of Electric Machines*. Springer International Publishing, Cham, Switzerland. doi:10.1007/978-3-030-34758-1.

Luo, J., Zhuang, J., Jin, M., Xu, F., and Su, Y. (2024). An energy-efficient path planning method for unmanned surface vehicle in a time-variant maritime environment. *Ocean Eng.*, 301, 117544. doi:10.1016/j.oceaneng.2024.117544.

Prevljak, N.H. (2025). Germany's first all-electric ferry delivered. *Offshore Energy*.

Skjetne, R. (2005). *The Maneuvering Problem*. Ph.D. thesis, Norwegian University of Science and Technology, Faculty of Information Technology, Mathematics,and Electrical Engineering, ISBN 82-471-6859-6.

Skulstad, R., Li, G., Fossen, T.I., and Zhang, H. (2023). Constrained control allocation for dynamic ship positioning using deep neural network. *Ocean Eng.*, 279, 114434. doi:10.1016/j.oceaneng.2023.114434.

Suo, Y., Chen, X., Yue, J., Yang, S., and Claramunt, C. (2024). An Improved Artificial Potential Field Method for Ship Path Planning Based on Artificial Potential Field—Mined Customary Navigation Routes. *J. Mar. Sci. Eng.*, 12(5), 731. doi:10.3390/jmse12050731.

Teong-Beng Koay, M.C. (2013). Energy-efficient path planning for fully propelled AUVs in congested coastal waters. *Published in: 2013 MTS/IEEE OCEANS - Bergen*, 10–14. doi:10.1109/OCEANS-Bergen.2013.6608168.

Torben, T.R., Brodtkorb, A.H., and Sørensen, A.J. (2019). Control allocation for double-ended ferries with full-scale experimental results. *IFAC-PapersOnLine*, 52(21), 45–50. doi:10.1016/j.ifacol.2019.12.281.

Wang, Z. and Im, N. (2024). Enhanced artificial potential field for MASS's path planning navigation in restricted waterways. *Appl. Ocean Res.*, 149, 104052. doi:10.1016/j.apor.2024.104052.

Zhu, J., Shen, H., Tang, Q., Qin, Z., and Yu, Y. (2025). Energy-Efficient Route Planning Method for Ships Based on Level Set. *Sensors*, 25(2), 381. doi:10.3390/s25020381.